ACS NANO
Cite This: ACS Nano 2017, 11, 10273-10280
www.acsnano.org

ARTICLE

# Transparent Large-Area $MoS_2$ Phototransistors with Inkjet-Printed Components on Flexible Platforms

Tae-Young Kim,[†,#] Jewook Ha,[‡,#] Kyungjune Cho,[†] Jinsu Pak,[†] Jiseok Seo,[‡] Jongjang Park,[‡] Jae-Keun Kim,[†] Seungjun Chung,[*,†] Yongtaek Hong,[*,‡] and Takhee Lee[*,†]

[†]Department of Physics and Astronomy, and Institute of Applied Physics, and [‡]Department of Electrical and Computer Engineering, Inter-university Semiconductor Research Center (ISRC), Seoul National University, Seoul, 08826, Korea

Supporting Information

**ABSTRACT:** Two-dimensional (2D) transition-metal dichalcogenides (TMDCs) have gained considerable attention as an emerging semiconductor due to their promising atomically thin film characteristics with good field-effect mobility and a tunable band gap energy. However, their electronic applications have been generally realized with conventional inorganic electrodes and dielectrics implemented using conventional photolithography or transferring processes that are not compatible with large-area and flexible device applications. To facilitate the advantages of 2D TMDCs in practical applications, strategies for realizing flexible and transparent 2D electronics using low-temperature, large-area, and low-cost processes should be developed. Motivated by this challenge, we report fully printed transparent chemical vapor deposition (CVD)-synthesized monolayer molybdenum disulfide ($MoS_2$) phototransistor arrays on flexible polymer substrates. All the electronic components, including dielectric and electrodes, were directly deposited with mechanically tolerable organic materials by inkjet-printing technology onto transferred monolayer $MoS_2$, and their annealing temperature of <180 °C allows the direct fabrication on commercial flexible substrates without additional assisted-structures. By integrating the soft organic components with ultrathin $MoS_2$, the fully printed $MoS_2$ phototransistors exhibit excellent transparency and mechanically stable operation.

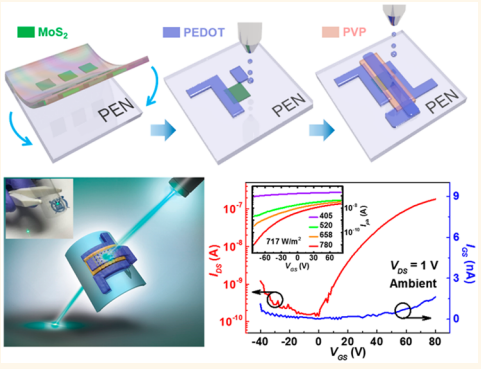


**KEYWORDS:** *$MoS_2$, chemical vapor deposition, inkjet-printing, phototransistor, flexible devices*

In recent years, two-dimensional (2D) transition metal dichalcogenides (TMDCs) have attracted considerable attention as an emerging semiconductor for realizing field-effect transistor (FET), sensor, and optoelectronic applications due to their atomic thickness, high surface-to-volume ratio, tunable band gap, *etc.*[1−7] Specifically, ultrathin monolayer molybdenum disulfide ($MoS_2$) is one of the promising channel materials in optoelectronics devices, such as photosensors, photodetectors, and photodiodes.[8−15] However, it is still difficult to produce large-area monolayer TMDC films, by widely used top-down methods, such as mechanical exfoliation,[16] thinning,[17] and liquid intercalation.[18] In this regard, many bottom-up synthesis methods, including metal−organic chemical vapor deposition (MOCVD),[19] physical vapor deposition (PVD),[20] and atomic layer deposition (ALD)[21] have been reported to realize large-area optoelectronic devices. Among these candidates, the one-step chemical vapor deposition (CVD) method has been widely used to yield high-quality and large-area $MoS_2$ films.[22−24] CVD-synthesized $MoS_2$ films allow atomically thin, uniform, and large-area semiconducting properties with a direct band gap energy of 1.9 eV[22−24] and thus offer promising opportunities in high-performance wearable optoelectronics.

However, other electronic components, including electrodes and dielectric layers, have been typically deposited with inorganic materials using ALD, thermal evaporation, and electron beam evaporation,[11−16] which are not compatible with large-area flexible platforms. Specifically, unnecessary procedures, such as a photoresist deposition or ultraviolet exposure, can degrade the electrical characteristics of $MoS_2$ channel layers. Recently, the use of graphene electrodes or hexagonal boron nitride dielectric layers to introduce dangling-bond free interfaces on $MoS_2$ has been suggested.[25,26] However, these layers require complicated and time-consuming etching and transferring processes with additional supporting layers. Therefore, an approach to implement functional layers

Received: July 12, 2017
Accepted: August 25, 2017
Published: August 25, 2017




DOI: 10.1021/acsnano.7b04893
ACS Nano 2017, 11, 10273−10280

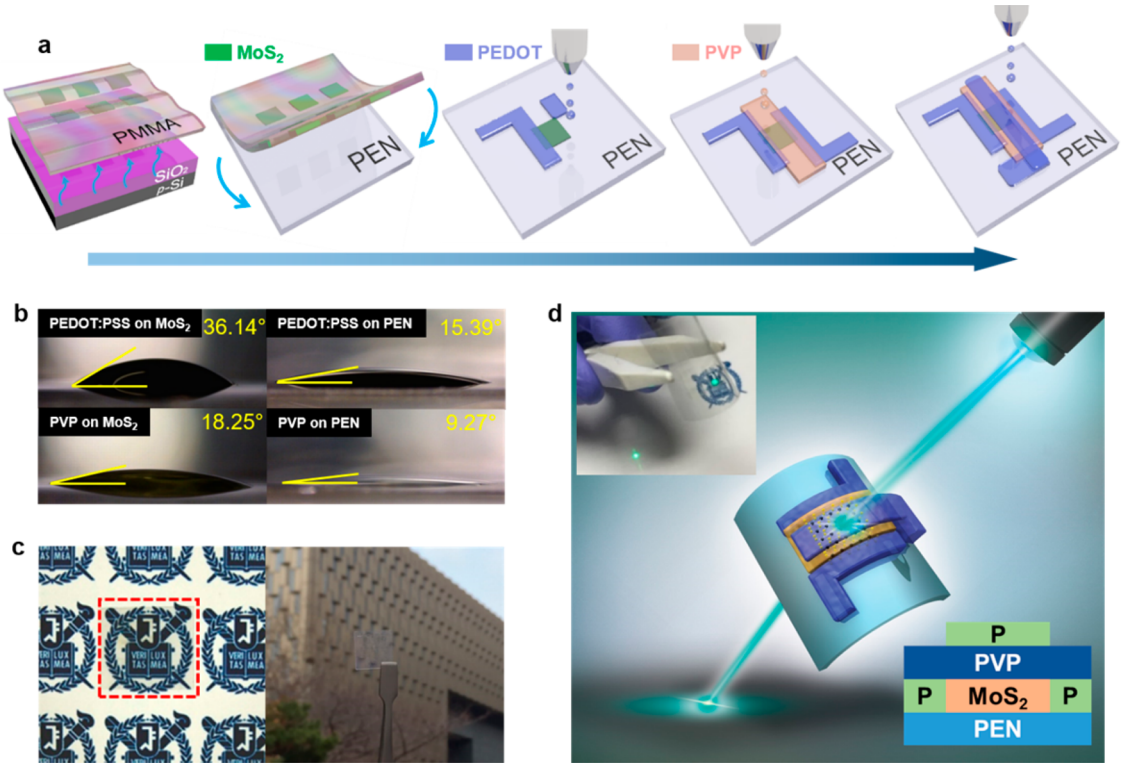


**Figure 1. (a) Schematic illustration of the fabrication processes for fully printed, flexible, and transparent CVD-synthesized $MoS_2$ phototransistors. (b) Contact angle measurements of PEDOT:PSS (top) and PVP (bottom) ink on the $MoS_2$ film (left) and PEN substrate (right). (c) Digital images of the transparent $MoS_2$ phototransistor arrays. In the left image, the device arrays (marked with a red square) were placed on a piece of paper with university symbols. The right image was taken in front of a building. (d) Photographic image (inset) and schematic of the devices under laser illumination. The 'P' indicates the PEDOT:PSS gate and source/drain electrodes. Seoul National University logo reprinted with permission.**

on flexible platforms is highly desirable for large-area $MoS_2$ applications. Furthermore, to fully utilize the excellent transparency and flexibility of monolayer $MoS_2$, the use of transparent organic materials is an attractive strategy to implement electronic components on flexible platforms.

Herein we fabricated flexible and transparent $MoS_2$ phototransistor arrays with all-organic components using drop-on-demand inkjet-printing technology. The CVD-synthesized monolayer $MoS_2$ channel layers were transferred onto flexible and transparent substrates using a polymer-assisted transfer method. Highly transparent organic electrodes and dielectric layers were directly deposited on the defined $MoS_2$ channel layer using cost-effective inkjet-printing technology without masks or assisted layers.[27−30] By integrating ultrathin $MoS_2$ and mechanically tolerable organic layers, the printed transparent phototransistors exhibited good stability under repetitive bending cycle tests. By conducting the carefully optimized printing processes, the fabricated fully printed phototransistors exhibited comparable photocharacteristics, including photoresponsivity and external quantum efficiency (EQE), to those of previously reported phototransistors with inorganic components fabricated by conventional photolithographic processes on rigid $SiO_2$/Si substrates.

## RESULTS AND DISCUSSION

Figure 1a schematically illustrates the device fabrication processes. First, a large-area monolayer $MoS_2$ film was synthesized with $MoO_3$ and sulfur (S) powders in the presence of Ar carrier gas.[30] The heating temperatures were 700 and 200 °C for $MoO_3$ and S powders, respectively. Then, the $MoS_2$ film synthesized on the $SiO_2$/Si substrate was patterned using a reactive ion etching (RIE) system in an $O_2$ plasma. To define the channel region, the $MoS_2$ film was covered with a shadow mask. The patterned CVD-synthesized $MoS_2$ film was transferred onto a polyethylene−naphthalate (PEN) substrate using the poly(methyl methacrylate) (PMMA)-assisted transfer method.[31] After attaching thermal tape as a supporting layer, the entire structure (supporting tape/PMMA/$MoS_2$/$SiO_2$/Si) was immersed in a potassium hydroxide solution (~25%) to detach the $MoS_2$ film from the $SiO_2$/Si substrate. Then, all the other components, including dielectric and electrodes, were inkjet-printed onto the patterned $MoS_2$ array without any surface treatments under ambient conditions. Specifically, poly(3,4-ethylenedioxythiophene) polystyrenesulfonate (PEDOT:PSS) source/drain (S/D) electrodes, a cross-linked poly(4-vinylphenol) (PVP) gate dielectric layer, and a PEDOT:PSS top-gate electrode were sequentially inkjet-printed on the desired positions of the device substrate. The maximum processing temperature of 180 °C facilitated the direct integration of a wide range of printable organic materials onto the flexible substrate. It should be noted that the ultrathin $MoS_2$ channel layer was extremely sensitive to the surface roughness of underlying layers; therefore, a top-gate configuration was employed in this work because of the relatively poor surface roughness of the inkjet-printed PVP gate dielectric (rms roughness of ~4 nm) compared with that of the PEN substrate (rms roughness of ~1 nm). The contact properties of the PEDOT:PSS and PVP inks on the $MoS_2$ film and PEN substrate were optimized with a consideration of the ink


DOI: 10.1021/acsnano.7b04893
ACS Nano 2017, 11, 10273−10280

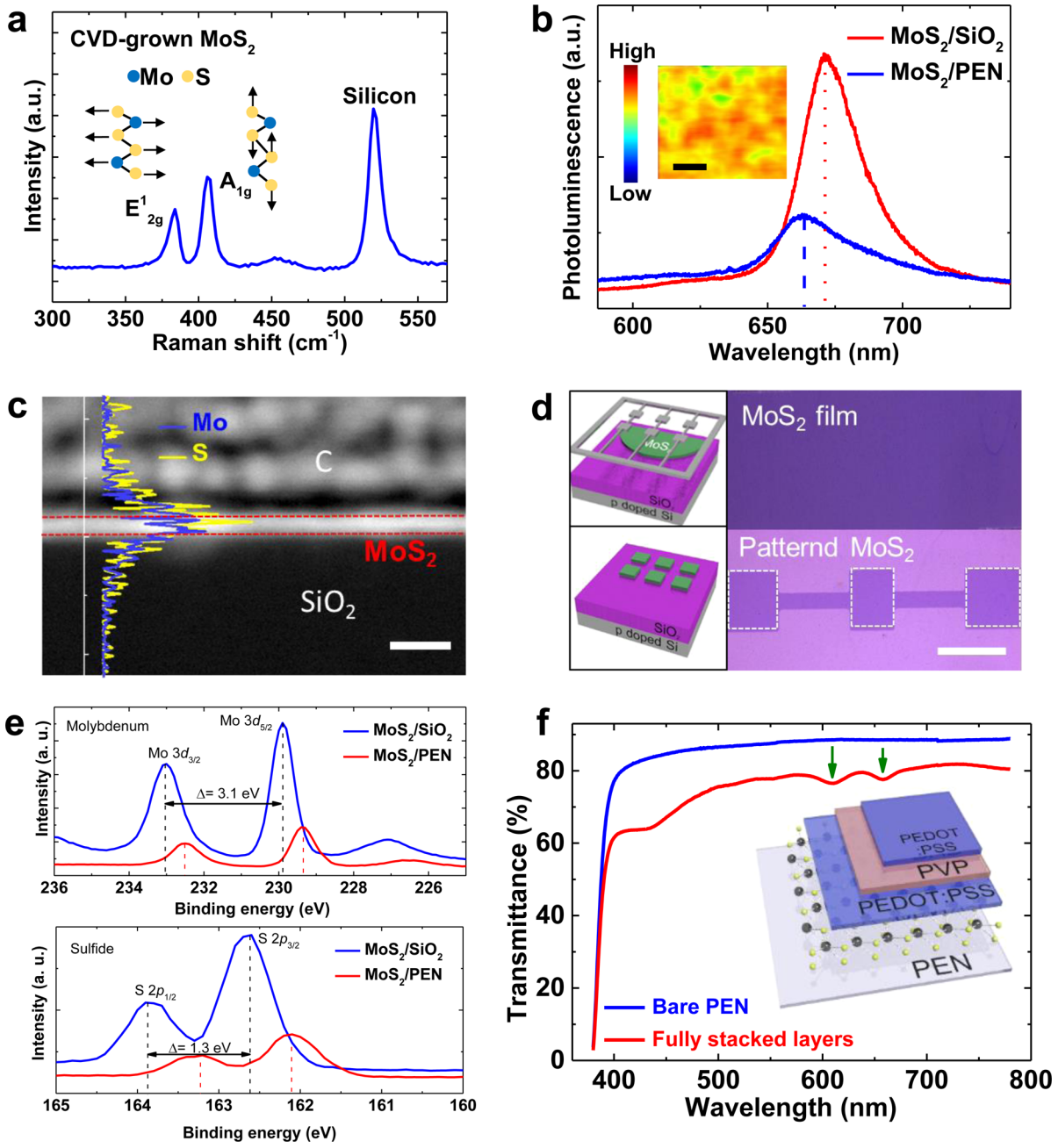


**Figure 2.** (a) Raman spectrum of a CVD-synthesized monolayer $MoS_2$ film on a $SiO_2$/Si substrate. (b) PL spectra of CVD-synthesized monolayer $MoS_2$ films on $SiO_2$/Si and PEN substrates. The inset shows a PL intensity mapping at 670 nm (=1.85 eV). Scale bar is 5 $\mu$m. (c) EDS data of Mo (blue line) and S (yellow line) and a cross-sectional STEM image of a CVD-synthesized $MoS_2$ film on a $SiO_2$/Si substrate. Scale bar is 5 nm. (d) Optical images of a CVD-synthesized $MoS_2$ channel before (top) and after (bottom) selective patterning processes. Scale bar is 400 $\mu$m. (e) XPS spectra of a CVD-synthesized monolayer $MoS_2$ film on a $SiO_2$/Si (top) substrate and transferred $MoS_2$ film on the PEN (bottom) substrate. (f) Transmittance spectra of a bare PEN substrate (blue line) and fully stacked films (red line). Inset shows the schematic of the stacked layers (PEDOT:PSS/PVP/PEDOT:PSS/$MoS_2$/PEN) of our devices.

chemistry that allowed well-defined printed layers while preventing undesirable dewetting issues on the underlying layers (Figure 1b). Owing to the use of ultrathin $MoS_2$ and transparent organic layers, the fully integrated phototransistors exhibited high transparency (Figure 1c). Photographic images of our devices are shown on a piece of paper (left, Figure 1c) and in front of a building (right, Figure 1c). In particular, the laser-light transmitted the entire device structure without reflection or scattering (Figure 1d).

The uniformity of the synthesized monolayer $MoS_2$ film on a $SiO_2$/Si substrate was evaluated by Raman and photoluminescence (PL) spectroscopy techniques. The Raman peak difference (~20.7 $cm^{-1}$) between in-plane $E^1_{2g}$ and out-of-plane $A_{1g}$ (Figure 2a) and a distinct PL peak A (~670 nm; ~1.85 eV) at the K point of the Brillouin zone (Figure 2b) provided evidence that the CVD-synthesized $MoS_2$ film is an uniformly grown monolayer.[11,12,32] Interestingly, the blue-shifted PL signal of the transferred $MoS_2$ film on the PEN substrate was observed due to a slight tensile strain that was



DOI: 10.1021/acsnano.7b04893
ACS Nano 2017, 11, 10273−10280

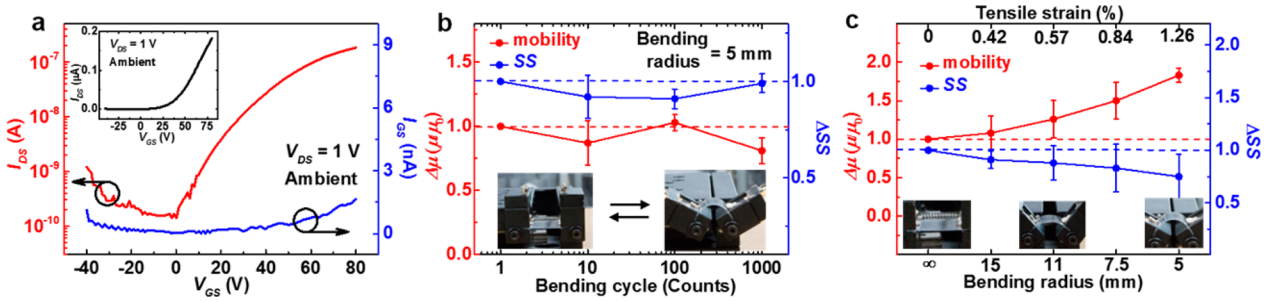


**Figure 3.** (a) $I_{DS}$−$V_{GS}$ curves using a log scale at $V_{DS}$ = 1 V. Inset represents the $I_{DS}$−$V_{GS}$ curves using a linear scale. The change in mobility ($\mu$) and subthreshold swing (SS) versus (b) number of bending cycles with a bending radius = 5 mm and (c) bending radii of 5, 7.5, 11, 15, and ∞.

induced in the $MoS_2$ layer during the CVD synthesis process because of the difference in thermal expansion coefficients of the $SiO_2$/Si and $MoS_2$ layers.[33,34] For the further investigation, PL mapping over an area of 20 $\mu$m × 20 $\mu$m was performed, as shown in the inset of Figure 2b. The color distribution indicated that the CVD-synthesized $MoS_2$ channel layer has uniform band gap energy at 1.85 eV. Cross-sectional scanning transmission electron microscopy (STEM) with energy dispersive X-ray spectroscopy (EDS) also supported that the $MoS_2$ layer was uniformly synthesized showing confined Mo and S signals (Figure 2c). To implement phototransistor arrays, the $MoS_2$ film was selectively patterned using RIE in an $O_2$ plasma (Figure 2d). Note that the CVD-synthesized monolayer $MoS_2$ film typically has a dark violet color on 270 nm-thick $SiO_2$.[24,30,32] The white-dashed rectangles indicate the patterned $MoS_2$ channels after the RIE process. By exploiting the optimized PMMA-assisted transfer method, the patterned CVD-synthesized $MoS_2$ array was successfully transferred onto a PEN substrate without physical damage. The transferred patterned $MoS_2$ array films on the PEN substrate maintained its structural quality (Figure 2b,e); however, relatively weak PL and X-ray photoelectron spectroscopy (XPS) signals were observed because of light scattering from the PEN substrates. The XPS spectra depicted in Figure 2e indicate the binding energies of the Mo 3d and S 2p orbitals (229.9, 233, 162.6, and 163.9 eV for Mo $3d_{5/2}$, Mo $3d_{3/2}$, S $2p_{3/2}$, and S $2p_{1/2}$, respectively). The difference between the binding energies of each orbital (3.1 and 1.3 eV for Mo 3d and S 2p, respectively) were consistent with the previously reported values[24] of CVD-synthesized monolayer $MoS_2$. In addition, the S/Mo atomic ratio of 1.95 estimated from the XPS, suggests that our synthesized $MoS_2$ film is stoichiometric. The lower binding energy of transferred $MoS_2$ film originated from the transferring process. The fully printed $MoS_2$ phototransistors with organic materials showed a high transmittance over 76% in the visible wavelength range, whereas the bare PEN substrate exhibited a transmittance of ∼87% in the same wavelength range (Figure 2f). Noticeable absorption peaks at 1.87 and 2.02 eV (marked as arrows in Figure 2f) were observed. These peaks were attributed to the direct transition from the spin−orbit split valence band to the conduction band of $MoS_2$ monolayer, which is consistent with the previously reported results for both mechanically exfoliated[11,12] and CVD-synthesized $MoS_2$ monolayers.[35] In particular, the wavelength of the onset of the absorption should correspond to the band gap energy. The PEDOT:PSS and PVP layers evenly reduced the optical transmittance by ∼5% over the whole visible range. Because the fully transparent printed organic layers do not exhibit specific absorption peaks in the visible wavelength range, the photocharacteristics were entirely determined by the atomically thin $MoS_2$ channel layer without interference (Figure S1, Supporting Information, SI). To consider the worst-case in transmittance, the measured films were prepared by sequentially printing all phototransistor layers over the entire PEN substrate in the following order: $MoS_2$, PEDOT:PSS, PVP, and PEDOT:PSS on the PEN substrate (see the inset illustration of Figure 2f).

Figure 3a exhibits the transfer (source drain current versus gate voltage, $I_{DS}$−$V_{GS}$) characteristics of a fully printed $MoS_2$ phototransistor measured in air. In particular, the gate leakage ($I_{GS}$), which can cause significant interference in the photocurrent,[36] was greatly suppressed by removing the PMMA supporting layer very carefully and optimizing the inkjet-printing conditions for the PVP dielectric layer formation. These efforts were necessary because the hydrophobic PMMA residue causes a critical dewetting issue during the PVP printing process, resulting in a high gate to source leakage current. As a result, the gate leakage current was drastically suppressed to <1 nA after removing the PMMA layer with the optimized steps (Figure S3, SI). The extracted field-effect mobility in the linear regime ($\mu$) was found to be ∼0.27 $cm^2/V{\cdot}s$ using the following equation, $\mu = \left(\frac{\partial I_{DS}}{\partial V_{GS}}\right)\frac{L}{W}\frac{1}{C_i V_{DS}}$, where $\left(\frac{\partial I_{DS}}{\partial V_{GS}}\right)$, $L$, $W$, $C_i$, and $V_{DS}$ denote the transconductance, channel length, channel width, capacitance between the channel and gate per unit area. and source-drain voltage, respectively. The grain boundaries of the CVD-synthesized $MoS_2$ film,[23] the low-conductivity of the PEDOT:PSS electrode, and the low-$k$ PVP dielectric deteriorated the electrical performance of the fully printed CVD-grown $MoS_2$ phototransistors. Although the difference in the electron affinity of monolayer $MoS_2$ (∼4.0 eV) and the work function of the printed PEDOT:PSS layer (∼5.07 eV) (Figure S5, SI), resulted in a high Schottky barrier, an ohmic-like contact property was exhibited with a good linearity of $I_{DS}$ near low $V_{DS}$ due to the chemical reactions at the PEDOT:PSS/$MoS_2$ interfaces.[37] Furthermore, it should be noted that because the large-area $MoS_2$ channel also had a relatively high resistance due to the long-channel length of ∼100 $\mu$m and large number of $MoS_2$ grain boundaries on the film,[30] which resulted in an on-state current of ∼$10^{-7}$ A, the contact resistance of PEDOT:PSS with the $MoS_2$ channel (∼1.9 MΩ determined from the Y-function method,[38] Figure S10, SI) was acceptable.[39,40]

Owing to the use of soft organic materials, the electrical performance was not degraded during a mechanical stability test over 1000 repetitive bending-relaxation cycles at a bending



DOI: 10.1021/acsnano.7b04893
ACS Nano 2017, 11, 10273−10280

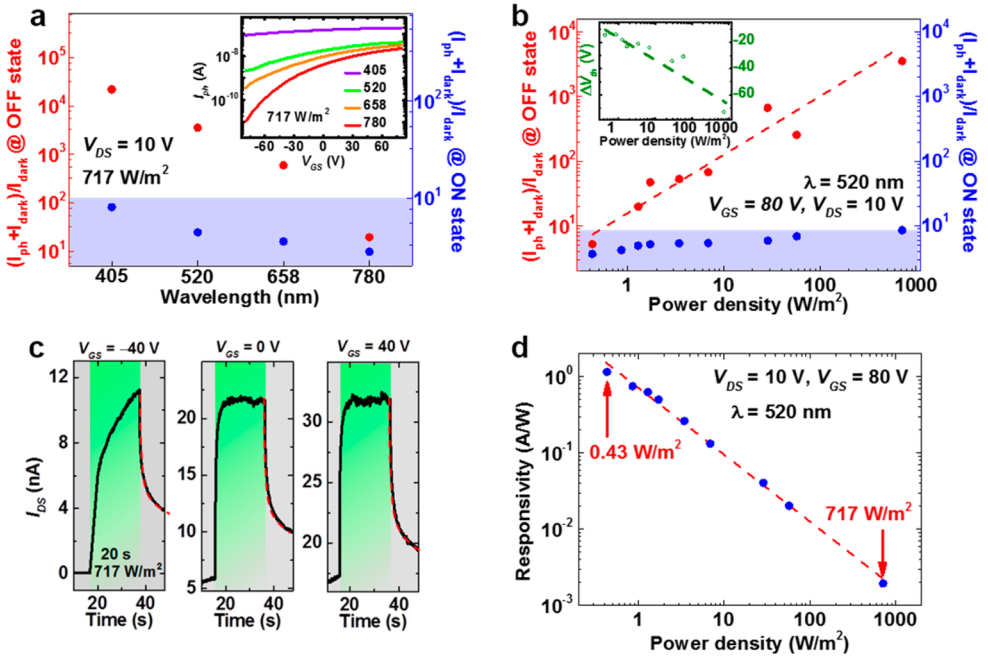


**Figure 4.** (a) The ratio of $I_{light}$ (= $I_{ph}$ + $I_{dark}$) to $I_{dark}$ in the ON and OFF states as a function of (a) wavelength and (b) laser power at a fixed $V_{DS}$ = 10 V. Insets of (a) and (b) exhibit $I_{ph}$ *versus* $V_{GS}$ and the change in $V_{th}$ with respect to the laser power, respectively. As the laser power increased, $V_{th}$ shifted in the negative voltage direction, which indicates an increase in $I_{ph}$ in the subthreshold regime. (c) Time-resolved photocurrent measurement under laser illumination ($\lambda$ = 520 nm). The green-shaded regions indicate laser illumination for 20 s. (d) Responsivity of phototransistors as a function of power density under laser illumination ($\lambda$ = 520 nm).

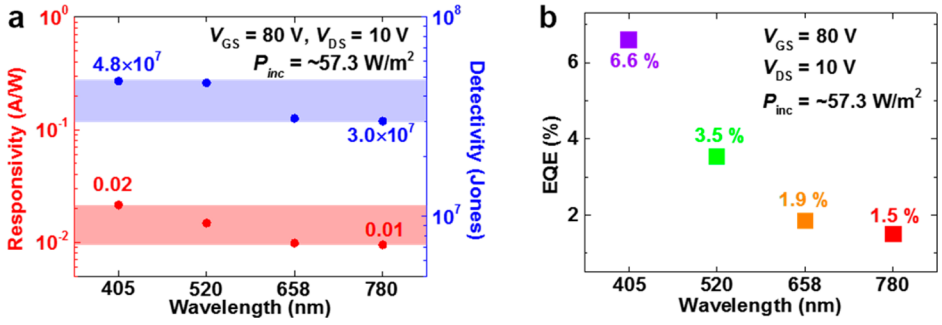


**Figure 5.** (a) Photoresponsivity, photodetectivity, and (b) external quantum efficiency as a function of wavelength at a fixed $V_{GS}$ = 80 V, $V_{DS}$ = 10 V, and laser power density = 57.3 W/m$^2$.

radius ($R$) of 5 mm, which corresponds to a uniaxial tensile strain of 1.26% along the channel length (Figure S11, SI) (Figure 3b). The atomically thin $MoS_2$ layer allowed superior durability under a mechanical strain of 11% compared with widely used engineering materials, such as carbon nanotubes and oxide-based semiconductors.[41,42] In contrast to the good mechanical stability under repetitive bending cycles, the $\mu$ and subthreshold swing (SS) measured in a bent state ($R$ of 15 mm, 11 mm, 7.5 mm, and 5 mm) increased as $R$ decreased (Figure 3c). These enhancements can be attributed to a reduction in the band gap energy of CVD-synthesized $MoS_2$ when mechanically deformed (Figure S12, SI).[6,34,41,43]

Figure 4 shows the photocharacteristics of the $MoS_2$ phototransistors under laser illumination. The measurements were executed after the devices were maintained on a 400 K hot-chuck in vacuum for 20 h to provide successfully suppressed $I_{GS}$ by eliminating adsorbed water and oxygen molecules on the $MoS_2$ and gate dielectric layers. To investigate the contribution of the photocurrent ($I_{light}$ = $I_{ph}$+ $I_{dark}$) to $I_{DS}$, the ratio of $I_{light}$ to $I_{dark}$ in ON and OFF states was measured for different wavelengths with a fixed laser power density of 717 W/m$^2$ at $V_{DS}$ = 10 V (Figure 4a). The ON and OFF states are measured at $V_{GS}$ = 80 and −80 V, respectively. Under laser illumination, the ratio in the OFF state drastically increased from ~10$^1$ to ~10$^4$, whereas in the ON state, the ratio was below 10 (see the blue-shaded region in Figure 4a).[44] In particular, the $I_{light}/I_{dark}$ ratio was increased from 10 to 1000 as a function of wavelength. An increase in the large $I_{ph}$ in the OFF state was observed in our study compared with that of the previously reported phototransistors with mechanically exfoliated $MoS_2$ due to the relatively large channel area ($W/L$ = 400 $\mu$m/100 $\mu$m).[14] This advantage of CVD-synthesized $MoS_2$ offers opportunities for large-area optoelectronics applications with a good photosensitivity. Moreover, the ratio of currents in the ON and OFF states also showed good linearity in the laser power density (ranging from 0.43 to 717 W/m$^2$ at $\lambda$ = 520 nm), which is an important characteristic for photosensor applications (Figure 4b).

The photodecay time ($\tau_{decay}$), which depends on $V_{GS}$, was also investigated by measuring the time-resolved photocurrent



DOI: 10.1021/acsnano.7b04893
ACS Nano 2017, 11, 10273−10280

before and after laser illumination for 20 s with $V_{GS}$ values of −40, 0, and 40 V at $\lambda$ = 520 nm (Figure 4c). The decay curves were fitted by a stretched exponential equation,

$$I_{DS} = I_{ph,intial} \exp\left[-\left(\frac{t}{\tau}\right)^{\beta}\right]$$

where $I_{ph,initial}$, $t$, $\beta$, and $\tau$ denote $I_{dark}$, time, the fitting parameter, and relaxation time, respectively. After laser illumination with a power density of 717 W/m$^2$, $\tau_{decay}$ decreased from 6.7 to 1.7 s as $V_{GS}$ increased from −40 to 40 V because the photocurrent contribution was weak at high $V_{GS}$, as previously mentioned. The shorter decay time compared with that of conventional CVD-synthesized $MoS_2$ phototransistors fabricated on a $SiO_2$/Si substrate is attributed to fewer interfacial traps between printed PVP dielectric and transferred $MoS_2$ layers.[14,45] It should be noted that the effect of interfacial traps produced at $MoS_2/SiO_2$ during the high-temperature CVD-synthesis for large-area $MoS_2$ films[46,47] could be suppressed by the release and transfer processes onto other substrates. The monotonic decrease in responsivity with increasing incident photopower indicates that the trap states of CVD-synthesized $MoS_2$ are saturated (Figure 4d).[8,45]

The responsivity and detectivity were also characterized for various laser wavelengths (Figure 5a). The fully transparent $MoS_2$ phototransistors exhibited comparable photoresponsivity and photodetectivity over the entire visible range from 400 to 800 nm compared with that of mechanically exfoliated $MoS_2$ phototransistors on opaque platforms.[48,49] Moreover, the wavelength-dependent external quantum efficiency (EQE) (up to ∼6.6%) also supports the fully printed transparent phototransistors, which exhibit good photocharacteristics, even though a top-gate configuration was employed (Figure 5b).[49] Note that the wavelength-dependent EQE is dominantly attributed to the absorbance peaks in the $MoS_2$ layer (Figure S1, SI). Also, despite the use of the inkjet-printed electrodes and dielectric and transfer-printed $MoS_2$, our flexible and transparent $MoS_2$ phototransistors showed reasonable photoresponsivity compared to some of the previously reported values (Figure 6).[9,44,48,49] Better photoresponsivity could be expected using a more optimized photocharacterization setup, for example laser density and the beam spot size of the laser.

## CONCLUSIONS

We have successfully demonstrated fully printed, transparent $MoS_2$ phototransistor arrays on flexible platforms. The CVD-synthesized monolayer $MoS_2$ and organic dielectric and electrode components were deposited directly onto flexible substrates using the optimized polymer-assisted transfer and inkjet-printing technologies, respectively. By employing ultrathin $MoS_2$ and transparent organic layers, the fully printed phototransistors exhibited excellent transparency and tolerance while maintaining electrical characteristics under tensile strain. Our work presents an opportunity to realize 2D TMDC-based low-cost wearable device applications beyond conventional electronics that employ brittle components.

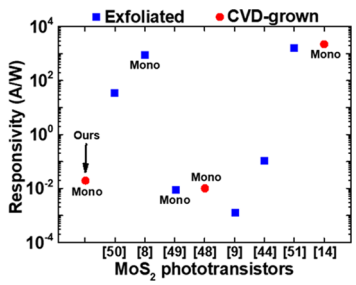


**Figure 6. Photoresponsivity of previously reported $MoS_2$ phototransistors. Values from refs 8, 9, 14, 44, and 48−51. The leftmost one is the value in this work.**

## METHODS

**$MoS_2$ Thin Film Synthesis.** A dual-heating zone CVD system was used for synthesizing monolayer $MoS_2$ films. Two crucibles were placed in a quartz tube. One crucible that contained the S powder (99.5%, Sigma-Aldrich) was heated to ∼200 °C, and the other crucible that contained the $MoO_3$ powder (99.98%, Sigma-Aldrich) and $SiO_2$ substrate was heated to ∼700 °C. Ar gas was used as a carrier gas.

**Inkjet-Printing for Organic Electrodes and Dielectric Layers Formation.** The patterned CVD-synthesized monolayer $MoS_2$ film was transferred onto a transparent and flexible PEN substrate. It should be noted that the expression, "fully printed" can be widely accepted from direct printing *via* nozzles to the polymer-assisted transfer methods. Then, all the other components, including transparent conductive polymer electrodes and dielectric layers, were deposited by an inkjet-printing technique without any surface treatment under ambient conditions. For the *S*/*D* electrode formation, a PEDOT:PSS ink (1 wt % in $H_2O$, Sigma-Aldrich) was inkjet-printed in one pass on the $MoS_2$-transferred PEN substrate with a drop spacing of 40 $\mu$m and a drop velocity of 10 m/s at room temperature using an inkjet printer (DMP-2831, Dimatix Corp., Fujifilm, USA). After printing, they were annealed at 130 °C for 30 min in an atmospheric environment. It should be noted that 2 wt % of fluorosurfactant Zonyl FS-300 (Sigma-Aldrich Corp.) was added to the PEDOT:PSS ink to improve both the conductivity and ability to withstand tensile strain.[52] The defined channel width and length were 400 and 100 $\mu$m, respectively. On the inkjet-printed PEDOT:PSS *S*/*D* electrodes and transfer-printed $MoS_2$ channel layer, a PVP solution, which contained 10 wt % of PVP powder ($M_w \approx 25\,000$) and 2 wt % of poly(melamine-*co*-formaldehyde) (PMFM) as a cross-linking agent dissolved in propylene glycol methyl ether acetate (PGMEA, ≥99.5%), was inkjet-printed in two passes with a drop spacing of 25 $\mu$m and a drop velocity of 8 m/s for the formation of a well-defined gate dielectric layer. To minimize the formation of pin holes on the surface of the cross-linked PVP gate dielectric, ramped curing (ramping at 5 °C/3 min and sequential soaking at 100 °C for 20 min and 180 °C for 30 min) was conducted.[53] Finally, for the gate electrode formation, the same PEDOT:PSS ink added to 2 wt % of Zonyl FS-300 (Sigma-Aldrich Corp.) was inkjet-printed onto the gate dielectric layer in two passes with the same printing and annealing conditions used for the formation of the *S*/*D* electrodes. The thicknesses of the device components were 125 $\mu$m, 1 $\mu$m, and 100−180 nm for the PEN substrate, PVP dielectric layer, and PEDOT:PSS contact electrodes, respectively.

**Optimization of PMMA Supporting Layer Removal Process.** The PMMA/$MoS_2$/PEN structure was immersed into 70 °C acetone and isopropyl alcohol for 2 h. Then, the structure was annealed in a tube furnace for 4 h with 100 sccm Ar gas flow rate, which corresponds to a few mTorr in pressure. Finally, the structure was immersed again into acetone at 70 °C for 1 h. It should be noted that the well-known PMMA eliminating methods that use ultraviolet oxygen exposure or reactive ion etching cannot be employed in this work because these treatments can easily physically damage the $MoS_2$ monolayer.

## ASSOCIATED CONTENT

### Supporting Information

The Supporting Information is available free of charge on the ACS Publications website at DOI: 10.1021/acsnano.7b04893.



DOI: 10.1021/acsnano.7b04893
ACS Nano 2017, 11, 10273−10280

Details on optical transmittance of the layer-by-layer stacked device structure, optimization of the PMMA supporting layer removal process, electrical and optical characteristics of the PEDOT:PSS electrode layer, device fabrication process, analysis of the contact properties of PEDOT:PSS electrodes using the *Y*-function method, investigation of applied mechanical strain of the printed phototransistors under bent conditions, band gap modulation of CVD-grown $MoS_2$ under bent conditions, and experimental conditions for evaluating the photocharacterization (PDF)

## AUTHOR INFORMATION


### Corresponding Authors

*E-mail: seungjun@phya.snu.ac.kr.
*E-mail: yongtaek@snu.ac.kr.
*E-mail: tlee@snu.ac.kr.

### ORCID

Takhee Lee: 0000-0001-5988-5219


### Author Contributions

#T.-Y.K. and J.H. contributed equally to this work.

### Notes

The authors declare no competing financial interest.

## ACKNOWLEDGMENTS

The authors appreciate the financial support of the National Creative Research Laboratory program (Grant No. 2012026372) through the National Research Foundation of Korea, funded by the Korean Ministry of Science and ICT. J.H. and Y.H. appreciate the financial support of the R&D Convergence Program (CAP-15-04-KITECH) of Korean National Research Council of Science & Technology and the Technology Innovation Program (10041957) funded by the Korean Ministry of Trade, Industry & Energy. T.-Y.K. and S.C. appreciate the support by the National Research Foundation of Korea (NRF) grant funded by the Korea government (MSIP; Ministry of Science, ICT & Future Planning) (NRF-2017R1C1B2002323).

## REFERENCES


(1) Wang, Q. H.; Kalantar-Zadeh, K.; Kis, A.; Coleman, J. N.; Strano, M. S. Electronics and Optoelectronics of Two-Dimensional Transition Metal Dichalcogenides. *Nat. Nanotechnol.* **2012**, *7*, 699−712.

(2) Chhowalla, M.; Shin, H. S.; Eda, G.; Li, L. J.; Loh, K. P.; Zhang, H. The Chemistry of Two-Dimensional Layered Transition Metal Dichalcogenide Nanosheets. *Nat. Chem.* **2013**, *5*, 263−275.

(3) Akinwande, D.; Petrone, N.; Hone, J. Two-dimensional Flexible Nanoelectronics. *Nat. Commun.* **2014**, *5*, 5678.

(4) Jariwala, D.; Sangwan, V. K.; Lauhon, L. J.; Marks, T. J.; Hersam, M. C. Emerging Device Applications for Semiconducting Two-Dimensional Transition Metal Dichalcogenides. *ACS Nano* **2014**, *8*, 1102−1120.

(5) Georgiou, T.; Jalil, R.; Belle, B. D.; Britnell, L.; Gorbachev, R. V.; Morozov, S. V.; Kim, Y.-J.; Gholinia, A.; Haigh, S. J.; Makarovsky, O.; Eaves, L.; Ponomarenko, L. A.; Geim, A. K.; Novoselov, K. S.; Mishchenko, A. Vertical Field-Effect Transistor Based on Graphene−$WS_2$ Heterostructures for Flexible and Transparent Electronics. *Nat. Nanotechnol.* **2013**, *8*, 100−103.

(6) Wu, W.; Wang, L.; Li, Y.; Zhang, F.; Lin, L.; Niu, S.; Chenet, D.; Zhang, X.; Hao, Y.; Heinz, T. F.; Hone, J.; Wang, Z. L. Piezoelectricity of Single-Atomic-Layer $MoS_2$ for Energy Conversion and Piezotronics. *Nature* **2014**, *514*, 470−474.

(7) Park, M.; Park, Y. J.; Chen, X.; Park, Y.-K.; Kim, M.-S.; Ahn, J.-H. $MoS_2$-Based Tactile Sensor for Electronic Skin Applications. *Adv. Mater.* **2016**, *28*, 2556−2562.

(8) Lopez-Sanchez, O.; Lembke, D.; Kayci, M.; Radenovic, A.; Kis, A. Ultrasensitive Photodetectors Based on Monolayer $MoS_2$. *Nat. Nanotechnol.* **2013**, *8*, 497−501.

(9) Perea-López, N.; Lin, Z.; Pradhan, N. R.; Iñiguez-Rábago, A.; Laura Elías, A.; McCreary, A.; Lou, J.; Ajayan, P. M.; Terrones, H.; Balicas, L.; Terrones, M. CVD-grown Monolayered $MoS_2$ as an Effective Photosensor Operating at Low-Voltage. *2D Mater.* **2014**, *1*, 011004.

(10) Venkata Subbaiah, Y.; Saji, K.; Tiwari, A. Atomically Thin $MoS_2$: A Versatile Nongraphene 2D Material. *Adv. Funct. Mater.* **2016**, *26*, 2046−2069.

(11) Mak, K. F.; Lee, C.; Hone, J.; Shan, J.; Heinz, T. F. Atomically Thin $MoS_2$: A New Direct-Gap Semiconductor. *Phys. Rev. Lett.* **2010**, *105*, 136805.

(12) Splendiani, A.; Sun, L.; Zhang, Y.; Li, T.; Kim, J.; Chim, C.-Y.; Galli, G.; Wang, F. Emerging Photoluminescence in Monolayer $MoS_2$. *Nano Lett.* **2010**, *10*, 1271−1275.

(13) Lee, H. S.; Min, S.-W.; Chang, Y.-G.; Park, M. K.; Nam, T.; Kim, H.; Kim, J. H.; Ryu, S.; Im, S. $MoS_2$ Nanosheet Phototransistors with Thickness-Modulated Optical Energy Gap. *Nano Lett.* **2012**, *12*, 3695−3700.

(14) Zhang, W.; Huang, J.-K.; Chen, C.-H.; Chang, Y.-H.; Cheng, Y.-J.; Li, L.-J. High-Gain Phototransistors Based on a CVD $MoS_2$ Monolayer. *Adv. Mater.* **2013**, *25*, 3456−3461.

(15) Amani, M.; Lien, D.-H.; Kiriya, D.; Xiao, J.; Azcatl, A.; Noh, J.; Madhvapathy, S. R.; Addou, R.; Kc, S.; Dubey, M.; Cho, K.; Wallace, R. M.; Lee, S.-C.; He, J.-H.; Ager, J. W.; Zhang, X.; Yablonovitch, E.; Javey, A. Near-Unity Photoluminescence Quantum Yield in $MoS_2$. *Science* **2015**, *350*, 1065−1068.

(16) Radisavljevic, B.; Radenovic, A.; Brivio, J.; Giacometti, V.; Kis, A. Single-Layer $MoS_2$ Transistors. *Nat. Nanotechnol.* **2011**, *6*, 147−150.

(17) Castellanos-Gomez, A.; Barkelid, M.; Goossens, A. M.; Calado, V. E.; van der Zant, H. S. J.; Steele, G. Laser-Thinning of $MoS_2$: On Demand Generation of a Single-Layer Semiconductor. *Nano Lett.* **2012**, *12*, 3187−3192.

(18) Eda, G.; Yamaguchi, H.; Voiry, D.; Fujita, T.; Chen, M.; Chhowalla, M. Photoluminescence from Chemically Exfoliated $MoS_2$. *Nano Lett.* **2011**, *11*, 5111−5116.

(19) Kang, K.; Xie, S.; Huang, L.; Han, Y.; Huang, P. Y.; Mak, K. F.; Kim, C. J.; Muller, D.; Park, J. High-Mobility Three-Atom-Thick Semiconducting Films With Wafer-Scale Homogeneity. *Nature* **2015**, *520*, 656−660.

(20) Muratore, C.; Hu, J. J.; Wang, B.; Haque, M. A.; Bultman, J. E.; Jespersen, M. L.; Shamberger, P. J.; McConney, M. E.; Naguy, R. D.; Voevodin, A. A. Continuous Ultra-Thin $MoS_2$ Films Grown by Low-Temperature Physical Vapor Deposition. *Appl. Phys. Lett.* **2014**, *104*, 261604.

(21) Tan, L. K.; Liu, B.; Teng, J. H.; Guo, S.; Low, H. Y.; Loh, K. P. Atomic Layer Deposition of a $MoS_2$ Film. *Nanoscale* **2014**, *6*, 10584−10588.

(22) Lee, Y.-H.; Zhang, X.-Q.; Zhang, W.; Chang, M.-T.; Lin, C.-T.; Chang, K.-D.; Yu, Y.-C.; Wang, J. T.-W.; Chang, C.-S.; Li, L.-J.; Lin, T.-W. Synthesis of Large-Area $MoS_2$ Atomic Layers with Chemical Vapor Deposition. *Adv. Mater.* **2012**, *24*, 2320−2325.

(23) Dumcenco, D.; Ovchinnikov, D.; Marinov, K.; Sanchez, O. L.; Krasnozhon, D.; Chen, M.-W.; Gillet, P.; Morral, A.; Radenovic, A.; Kis, A.; Lazic, P.; Gibertini, M.; Marzari, N.; Kung, Y.-C.; Bertolazzi, S. Large-Area Epitaxial Monolayer $MoS_2$. *ACS Nano* **2015**, *9*, 4611−4620.

(24) Park, W.; Baik, J.; Kim, T. Y.; Cho, K.; Hong, W. K.; Shin, H. J.; Lee, T. Photoelectron Spectroscopic Imaging and Device Applications of Large-Area Patternable Single-Layer $MoS_2$ Synthesized by Chemical Vapor Deposition. *ACS Nano* **2014**, *8*, 4961−4968.

(25) Das, S.; Gulotty, R.; Sumant, A. V.; Roelofs, A. All Two-Dimensional, Flexible, Transparent, and Thinnest Thin Film Transistor. *Nano Lett.* **2014**, *14*, 2861−2866.




DOI: 10.1021/acsnano.7b04893
*ACS Nano* 2017, 11, 10273−10280

(26) Lee, G.-H.; Yu, Y.-J.; Cui, X.; Petrone, N.; Lee, C.-H.; Choi, M. S.; Lee, D.-Y.; Lee, C.; Yoo, W. J.; Watanabe, K.; Taniguchi, T.; Nuckolls, C.; Kim, P.; Hone, J. Flexible and Transparent $MoS_2$ Field-Effect Transistors on Hexagonal Boron Nitride-Graphene Heterostructures. *ACS Nano* **2013**, *7*, 7931−7936.
(27) Sekitani, T.; Nakajima, H.; Maeda, H.; Fukushima, T.; Aida, T.; Hata, K.; Someya, T. Stretchable Active-Matrix Organic Light-Emitting Diode Display Using Printable Elastic Conductors. *Nat. Mater.* **2009**, *8*, 494−499.
(28) Kim, B.; Jang, S.; Geier, M. L.; Prabhumirashi, P. L.; Hersam, M. C.; Dodabalapur, A. High-Speed, Inkjet-Printed Carbon Nanotube/Zinc Tin Oxide Hybrid Complementary Ring Oscillators. *Nano Lett.* **2014**, *14*, 3683−3687.
(29) Sekitani, T.; Takamiya, M.; Noguchi, Y.; Nakano, S.; Kato, Y.; Sakurai, T.; Someya, T. A Large-Area Wireless Power Transmission Sheet Using Printed Organic Transistors and Plastic Mems Switches. *Nat. Mater.* **2007**, *6*, 413−417.
(30) Kim, T.-Y.; Amani, M.; Ahn, G. H.; Song, Y.; Javey, A.; Chung, S.; Lee, T. Electrical Properties of Synthesized Large-Area $MoS_2$ Field-Effect Transistors Fabricated with Inkjet-Printed Contacts. *ACS Nano* **2016**, *10*, 2819−2826.
(31) Jiao, L. Y.; Fan, B.; Xian, X. J.; Wu, Z. Y.; Zhang, J.; Liu, Z. F. Creation of Nanostructures with Poly(methyl methacrylate)-Mediated Nanotransfer Printing. *J. Am. Chem. Soc.* **2008**, *130*, 12612−12613.
(32) Schmidt, H.; Wang, S.; Chu, L.; Toh, M.; Kumar, R.; Zhao, W.; Castro Neto, A. H.; Martin, J.; Adam, S.; Ö zyilmaz, B.; Eda, G. Transport Properties of Monolayer $MoS_2$ Grown by Chemical Vapor Deposition. *Nano Lett.* **2014**, *14*, 1909−1913.
(33) Amani, M.; Chin, M. L.; Mazzoni, A. L.; Burke, R. A.; Najmaei, S.; Ajayan, P. M.; Lou, J.; Dubey, M. Growth-Substrate Induced Performance Degradation in Chemically Synthesized Monolayer $MoS_2$ Field Effect Transistors. *Appl. Phys. Lett.* **2014**, *104*, 203506.
(34) Conley, H. J.; Wang, B.; Ziegler, J. I.; Haglund, R. F.; Pantelides, S. T.; Bolotin, K. I. Bandgap Engineering of Strained Monolayer and Bilayer $MoS_2$. *Nano Lett.* **2013**, *13*, 3626−3630.
(35) Mukherjee, B.; Tseng, F.; Gunlycke, D.; Amara, K.; Eda, G.; Simsek, E. Complex Electrical Permittivity of the Monolayer Molybdenum Disulfide ($MoS_2$) in Near UV and Visible. *Opt. Mater. Express* **2015**, *5*, 447−455.
(36) Yu, W. J.; Liu, Y.; Zhou, H.; Yin, A.; Li, Z.; Huang, Y.; Duan, X. Highly Efficient Gate-Tunable Photocurrent Generation in Vertical Heterostructures of Layered Materials. *Nat. Nanotechnol.* **2013**, *8*, 952−958.
(37) McDonnell, S.; Addou, R.; Buie, C.; Wallace, R. M.; Hinkle, C. L. Defect-Dominated Doping and Contact Resistance in $MoS_2$. *ACS Nano* **2014**, *8*, 2880−2888.
(38) Chang, H.-Y.; Zhu, W.; Akinwande, D. On the Mobility and Contact Resistance Evaluation for Transistors Based on $MoS_2$ or Two-Dimensional Semiconducting Atomic Crystals. *Appl. Phys. Lett.* **2014**, *104*, 113504.
(39) Sirringhaus, H.; Kawase, T.; Friend, R. H.; Shimoda, T.; Inbasekaran, M.; Wu, W.; Woo, E. P. High-Resolution Inkjet Printing of All-Polymer Transistor Circuits. *Science* **2000**, *290*, 2123−2126.
(40) Lee, M. W.; Lee, M. Y.; Choi, J. C.; Park, J. S.; Song, C. K. Fine Patterning of Glycerol-Doped PEDOT:PSS on Hydrophobic PVP Dielectric with Ink Jet for Source and Drain Electrode of OTFTs. *Org. Electron.* **2010**, *11*, 854−859.
(41) Bertolazzi, S.; Brivio, J.; Kis, A. Stretching and Breaking of Ultrathin $MoS_2$. *ACS Nano* **2011**, *5*, 9703−9709.
(42) Park, K.; Lee, D.; Kim, B.; Jeon, H.; Lee, N.; Whang, D.; Lee, H.; Kim, Y.; Ahn, J.-H. Stretchable, Transparent Zinc Oxide Thin Film Transistors. *Adv. Funct. Mater.* **2010**, *20*, 3577−3582.
(43) Manzeli, S.; Allain, A.; Ghadimi, A.; Kis, A. Piezoresistivity and Strain-Induced Band Gap Tuning in Atomically Thin $MoS_2$. *Nano Lett.* **2015**, *15*, 5330−5335.
(44) Choi, W.; Cho, M. Y.; Konar, A.; Lee, J. H.; Cha, G.-B.; Hong, S. C.; Kim, S.; Kim, J.; Jena, D.; Joo, J.; Kim, S. High-Detectivity Multilayer $MoS_2$ Phototransistors with Spectral Response from Ultraviolet to Infrared. *Adv. Mater.* **2012**, *24*, 5832−5836.
(45) Furchi, M. M.; Polyushkin, D. K.; Pospischil, A.; Mueller, T. Mechanisms of Photoconductivity in Atomically Thin $MoS_2$. *Nano Lett.* **2014**, *14*, 6165−6170.
(46) Kim, T.-Y.; Song, Y.; Cho, K.; Amani, M.; Ho Ahn, G. H.; Kim, J.-K.; Pak, J.; Chung, S.; Javey, A.; Lee, T. Analysis of the Interface Characteristics of CVD-Grown Monolayer $MoS_2$ by Noise Measurements. *Nanotechnology* **2017**, *28*, 145702.
(47) Zhu, W.; Low, T.; Lee, Y.-H.; Wang, H.; Farmer, D. B.; Kong, J.; Xia, F.; Avouris, P. Electronic Transport and Device Prospects of Monolayer Molybdenum Disulphide Grown by Chemical Vapour Deposition. *Nat. Commun.* **2014**, *5*, 3087.
(48) Yin, Z.; Li, H.; Li, H.; Jiang, L.; Shi, Y.; Sun, Y.; Lu, G.; Zhang, Q.; Chen, X.; Zhang, H. Single-Layer $MoS_2$ Phototransistors. *ACS Nano* **2012**, *6*, 74−80.
(49) Li, Z.; Chen, J.; Dhall, R.; Cronin, B. S. Highly Efficient, High Speed Vertical Photodiodes Based on Few-Layer $MoS_2$. *2D Mater.* **2017**, *4*, 015004.
(50) Pak, J.; Jang, J.; Cho, K.; Kim, T.-Y.; Song, Y.; Hong, W.-K.; Min, M.; Lee, H.; Lee, T.; Kim, J.-K. Enhancement of Photodetection Characteristics of $MoS_2$ Field Effect Transistors using Surface Treatment with Copper Phthalocyanine. *Nanoscale* **2015**, *7*, 18780−18788.
(51) Zhang, Q.; Bao, W.; Gong, A.; Gong, T.; Ma, D.; Wan, J.; Dai, J.; Munday, J. N.; He, J.-H.; Zhang, D.; Hu, L. A Highly Sensitive, Highly Transparent, Gel-Gated $MoS_2$ Phototransistor on Biodegradable Nanopaper. *Nanoscale* **2016**, *8*, 14237−14242.
(52) Vosgueritchian, M.; Lipomi, D. J.; Bao, Z. Highly Conductive and Transparent PEDOT:PSS Films with a Fluorosurfactant for Stretchable and Flexible Transparent Electrodes. *Adv. Funct. Mater.* **2012**, *22*, 421−428.
(53) Chung, S.; Kim, S. O.; Kwon, S.-K.; Lee, C.; Hong, Y. All-Inkjet-Printed Organic Thin-Film Transistor Inverter on Flexible Plastic Substrate. *IEEE Electron Device Lett.* **2011**, *32*, 1134−1136.


DOI: 10.1021/acsnano.7b04893
*ACS Nano* 2017, 11, 10273−10280